Resistive Shaping of Interconnected Low-Voltage Microgrids Operating Under Distorted Voltages

Augusto M. S. Alonso, Danilo I. Brandao, Elisabetta Tedeschi, Fernando P. Marafao

***Abstract*—Beyond the impacting presence of non-linear loads, low-voltage microgrids also experience low energy efficiency and resonance phenomena when operating interconnected to a distribution grid that suffers from distorted voltages. This paper proposes a model-free control strategy capable of coordinating inverters existing within a dispatchable microgrid, allowing to operate it as a single-controllable entity that behaves like a resistor at selected harmonic frequencies. Such resistive shaping uses a centralized control architecture to steer inverters to distributively compensate reactive and harmonic currents, supporting active current sharing. Consequently, the microgrid point-of-common-coupling operates with a high power factor when the grid imposes distorted voltages. Additionally, if resonant components exist, the strategy supports harmonic resonance damping, which minimizes deterioration of voltage quality. For instance, comparative results show that, for the considered scenario, the proposed resistive shaping damps resonances up to 50% better than a previous approach that compensates harmonics using sinusoidal current synthesis. Simulation results carried out on a three-phase low-voltage microgrid testbench, considering three inverters, demonstrate the above-mentioned capabilities of the proposed approach. Experimental results based on a single-phase microgrid prototype comprising two inverters with two linear loads and one non-linear load validate the applicability of the method to real-life implementations.**

***Index Terms*—Distributed generation, harmonics, microgrids, power factor, resonance.**

I. Introduction

DISTORTED voltages and currents are important in low-voltage (LV) power systems since they lead to low energy efficiency and deterioration of power quality [1]. Such nonlinearities are, for instance, caused by the increasing presence of non-linear loads and can be propagated throughout the distribution systems [2]. Additionally, even small voltage distortions may trigger resonances [3] and lead the power system to instability [4]. This situation is particularly true for LV microgrids (MGs) operating islanded or when they are connected to a weak grid upstream. Notably, high penetration of inverters interfacing distributed energy resources (DERs) in such MGs contribute to triggering resonances [2].

Since MGs operate interconnected most of the time, unless a bulky power conditioner is purposely placed at their point-of-common-coupling (PCC) [5], the existing DERs need to be properly coordinated to operate under distorted voltages. Otherwise, reliable operation of DERs is not ensured, and adequate management of the MG as a single-controllable entity is not achieved. Thus, the development of strategies to steer DERs in MGs under distorted voltage conditions is important.

The coordination of inverters within MGs that present distorted voltages is found in literature, mostly taking advantage of droop control to improve voltage and current quality [6]-[8]. For instance, [6] presented the implementation of variable harmonic impedance loops, devised by positive resistances and negative inductances to achieve selective current sharing among DERs. In addition, upon the existence of harmonic resonances, the strategy allows for shifting the resonant bands to higher-order frequencies to improve the damping capability. Similarly, a resistive-capacitive output impedance method is proposed in [7]. It provides fast reactive power-sharing and mitigation of circulating currents and voltage resonances by voltage-controlled inverters. Such an approach is realized by taking the DERs' output currents and voltages as feed-forward terms in the virtual impedance loops. However, fine-tuning between the resistive and capacitive shaping of DERs is required to avoid triggering harmonic resonances or operating under excessive voltage drops. In [8], a direct output voltage control integrated into a virtual admittance strategy is devised. Ref. [8] provides damping of voltage distortion by limiting the impedance shaped by parallel DERs. Nevertheless, the above-mentioned approaches only consider DERs in islanded MGs, a different scenario from the one within this paper. Hence, they do not address MGs connected to an upstream weak grid that suffers from background voltage harmonics.

A droop-free approach is proposed in [9] to steer two parallel DERs locally. A hybrid voltage and current control is modeled, providing the compensation for distorted load currents and avoiding harmonic voltage amplification under distorted grid conditions. Although efficient, the method allocates one DER to compensate for load currents and the second to mitigate the interactions caused by the operation of the first inverter. Thus, no real power-sharing occurs among them. Additionally, load currents must be measured, which is not realistic for real applications in LV MGs with high dispersion of loads. In [10],

The authors are grateful to FAPESP (Grants 2017/24652-8, 2016/08645-9), and the NFR (Grant f261735/H30).

A. M. S. Alonso and F. P. Marafao are with the Group of Automation and Integrated Systems, São Paulo State University, Sorocaba, Brazil. (e-mail: augusto.alonso@unesp.br, fernando.marafao@unesp.br).

A. M. S. Alonso and E. Tedeschi are with the Department of Electric Power Engineering, Norwegian University of Science and Technology, Trondheim, Norway (e-mail: elisabetta.tedeschi@ntnu.no). E. Tedeschi is also with the Department of Industrial Engineering, University of Trento, Trento, Italy.

D. I. Brandao is with the Graduate Program in Electrical Eng., Federal University of Minas Gerais, Brazil (e-mail: dibrandao@ufmg.br).

the Fryze–Buchholz–Depenbrock theory is used to coordinate DERs to share reactive and harmonic currents under a decentralized method. However, the method is only applied to two DERs, relying on direct measurement of load currents. Besides, no considerations are given to harmonic resonances.

An MG operating interconnected is addressed in [2], on which DERs emulate virtual resistors to offer resonance damping or synthesizing virtual capacitors to compensate for voltage harmonic drops. Moreover, ref. [2] presents a trade-off between accuracy in harmonic current sharing and resonance damping performance and sensibility to changes in grid parameters. In [11], a master/slave strategy is proposed to share harmonic currents and smooth voltage resonances utilizing resistive active power filters. However, it only considers single-phase networks and does not support active power sharing.

It has been demonstrated in [3] and [12] that, for the purpose of local applications, compensation based on the concept of resistive load synthesis (RLS) shows more resonance damping capability than sinusoidal current synthesis (SCS). Besides, [13] showed that RLS-based compensation supports the damping of harmonic propagation throughout distribution grids. The RLS approach consists of targeting the mitigation of those current harmonics that are non-proportional to voltages. Thus, current waveforms resemble the voltage waveforms independent of distortion and/or unbalance (i.e., resistive behavior). Instead, SCS imposes sinusoidal currents regardless of voltage waveforms. Another direct consequence of these two approaches is that based on definitions from modern power theories [14]-[16], unity power factor (PF) (i.e., PF is the ratio between the active power and the absolute value of the complex power) is only achieved when currents are in-phase to voltages and present proportional waveforms. Thus, under distorted voltages, unity PF is only obtained by RLS methods. To the best of the authors' knowledge, no previous work has investigated an RLS approach based on the coordination of multiple DERs to selectively control harmonic currents at the PCC of an interconnected MG. Hence, the basis of this paper is set.

A. Paper Contributions and Organization

Considering the scenario of LV MGs operating connected to an upstream grid that suffers from distorted voltages, the contributions and novelties of this paper are four-fold:

- The development of a model-free and centralized coordinated control strategy, which steers DERs to achieve distributed compensation of reactive and harmonic currents under distorted voltages imposed by the upstream grid. The strategy controls the MG as a single-controllable entity, shaping it as a resistor at selected frequencies. Thus, the MG PCC can operate with high PF [14]-[16]. It is reinforced that unbalance compensation is out of scope in this paper;
- Such coordination strategy also supports active current sharing among DERs, which allows the MG to operate under full self-consumption mode [17], lessening the burden of power dispatch of the upstream grid, if desired;
- The strategy is based on the concept of RLS. Consequently, it avoids deterioration of voltage quality when resonances are triggered by interactions among line impedances, capacitor banks, and non-linear loads. The method handles resonance frequencies higher than the fundamental component of the grid voltage and lower than the bandwidth of the DERs' current controllers. Moreover, virtual impedance loops or decomposition of sequence components are not needed. Lastly, this paper demonstrates that distributed DERs compensating for harmonic currents based on RLS also provide more damping capability than the SCS concept;
- Experimental results of an MG operating under distorted voltages are shown to validate the applicability of the proposed control approach to real-life implementations.

The proposed RLS strategy presents a novel ancillary operation for grid-connected MGs, allowing them to behave as low-impedance circuits at selected harmonic frequencies, minimizing resonances and increasing the overall grid stiffness.

This paper is organized as follows. Section II describes the considered MG topology and the modeling of the considered DERs. The proposed coordinated control strategy is presented in Section III. Simulations and comparative results comprising several scenarios are shown in Section IV. Experimental results in Section V validate the feasibility of the control approach. Finally, conclusions summarize the findings of this paper.

II. Considered MG and Control Infrastructure

The scope of applying the proposed control strategy is the one of urban LV MGs, presenting several DERs interfaced by inverters. In addition, the presence of linear and non-linear loads that draw active, reactive, and harmonic currents are considered. As seen in Fig. 1, this electrical topology also considers a distribution transformer at the PCC that interconnects the MG to the upstream grid. Moreover, such a main grid may present voltage harmonics. It is assumed that the MG inherits a homogenous distribution of loads, DERs, and line impedances of low X/R ratio (i.e., < 1). As discussed in Section IV-B, a resonant load is also considered at the MG PCC to depict the possible occurrence of resonances. The CIGRE's LV testbench [18], shown in Fig. 1, represents an example of such an MG topology, considered here for simulations.

Concerning the control organization, the proposed strategy is formulated based on a centralized architecture that takes advantage of a low-bandwidth communication link to coordinate distributed DERs. Thus, a central controller (CC) is located at the PCC for monitoring operational and power quality conditions at its node (see Fig. 1) [19]. Additionally, the CC is responsible for processing a novel formulation of the coordinated control strategy, so-called Generalized Current-Based Control (GCBC) [20], which steers DERs under a model-free [21] approach. Consequently, utilizing control coefficients broadcasted to DERs (i.e., $\alpha_{h\parallel}$ and $\alpha_{h\perp}$, later explained in Section III-A), the MG operates under RLS mode.

A. Hierarchical Control Architecture of the MG

The proposed coordination strategy is devised by a three-layer hierarchical control, in which lower layers take priority over upper ones. The primary layer is responsible for the local control of each DER at their point of connection (PoC) (see Fig. 2(a)). This layer comprises the current, voltage, and other additional control loops that DERs may present. It does not rely on communications to comply with grid codes. For this paper, DERs are modeled by three-phase inverters with an LCL filter, as in Fig. 2(a). Their local control (i.e., current and dc-link voltage loop) is devised just as in [22]; thus, DERs operate under current-controlled mode with an active damping loop.

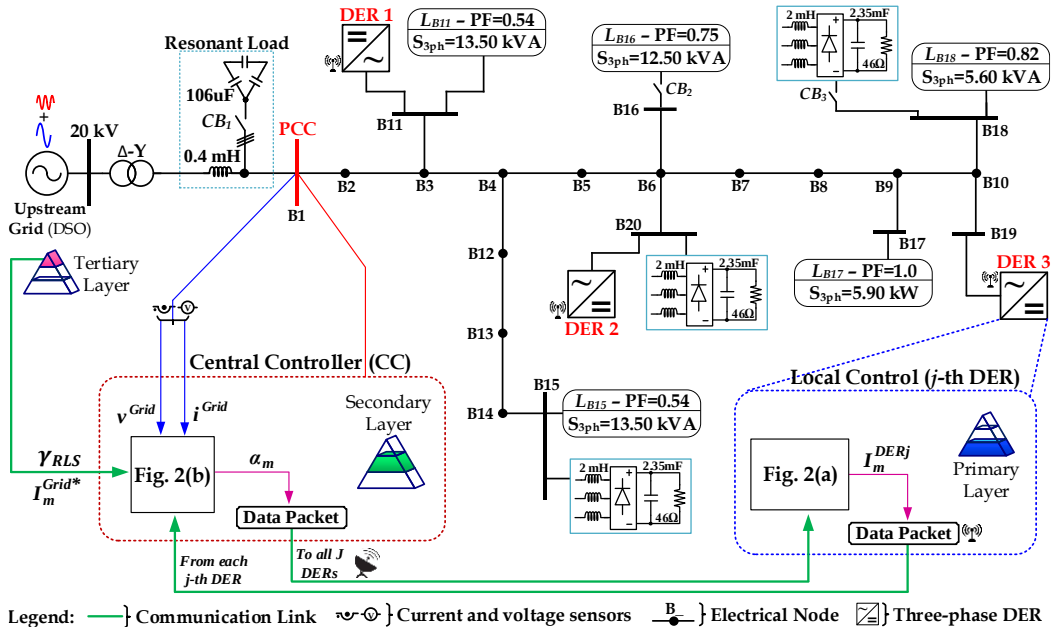

Fig. 1. Considered LV MG testbench based on [18], comprising loads and DERs, and adopted hierarchical control infrastructure from Section II-A.

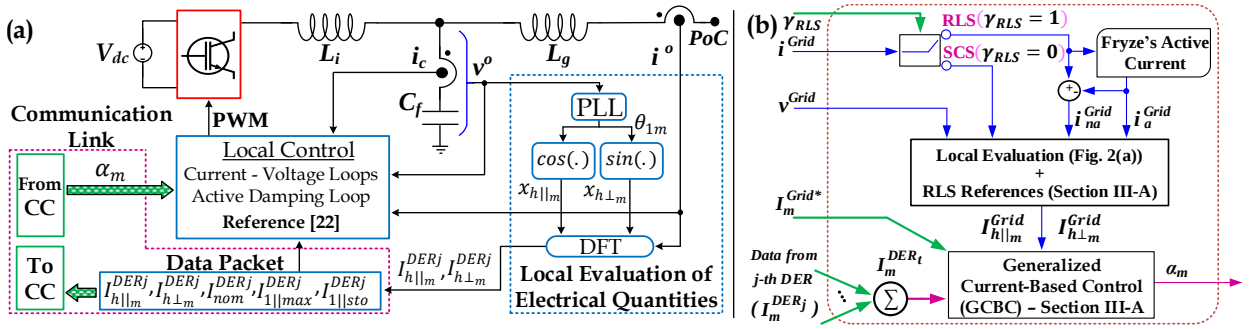

Fig. 2. (a) Single-phase equivalent circuit of a DER and primary layer of control; and (b) Proposed control approach implemented at the CC.

Secondary control is responsible for the coordinated operation of the inverters, being processed at the CC, as shown in Figs. 1 and 2(b). The GCBC algorithm is incorporated at this level, considering a modified implementation presented in Section III. The GCBC evaluates electrical quantities at the PCC. Also, it pulls and processes the status of DERs. Thus, it determines, as output, scaling coefficients for adjusting DERs' current injections. This concept is fairly different from hierarchical droop-based strategies, and additional details such as differences are presented in [23].

Finally, the third layer manages the interactions of the MG with the external agents (i.e., distribution system operator (DSO) and energy service providers). By receiving remote commands from the DSO (see Fig. 1), the CC coordinates DERs based on the GCBC to fulfill the requirements of power flow at the MG PCC. For what concerns this paper, the MG resistive shaping capability is commanded by the DSO. The variable γ_{RLS} sets this functionality, explained as follows.

III. Coordinated Control for Shaping Resistive MGs

One important feature of the GCBC is providing active, reactive, and harmonic current sharing among DERs. Such current sharing occurs proportionally to DERs' nominal capabilities, without knowledge of line impedances or the placement of DERs within the MG. Nonetheless, the GCBC strategy relies on an SCS concept. Thus, a modified implementation of the GCBC strategy is devised in this paper, striving for RLS-based coordination.

The variable γ_{RLS} commands the SCS and RLS functionalities for the MG. If grid voltages are distorted, the DSO sets $\gamma_{RLS} = 1$ at the CC, so the RLS approach is enabled. On the other hand, if $\gamma_{RLS} = 0$ is set, the SCS approach is offered. This circumstance occurs as seen in Fig. 2(b), where γ_{RLS} sets the selection of the current parcels that are processed by the GCBC, leading to different current sharing capabilities. Let us then consider the scenario in which the MG operates under distorted voltages imposed by the upstream grid. Herein, the subscript *m* stands for each phase of the three-phase system (i.e., *a*, *b*, *c*), and the superscripts "*Grid*" and "DER" stand for quantities measured at the PCC and DERs' PoCs, respectively.

For the SCS concept, if DERs share all the currents seen at the PCC (i.e., i_m^{Grid}) apart from the in-phase fundamental components ($i_{1||m}^{Grid}$), the PCC currents become sinusoidal. Thus, although current distortion is reduced, high PF is not achieved [14]-[16], and resonances may be amplified [3]. On the other hand, if the non-active current ($i_{na_m}^{Grid}$) is extracted from i_m^{Grid} (see Fig. 2(b)), only the reactive currents and the harmonic currents non-proportional to the voltages are obtained. This extraction occurs based on Fryze's active current definition ($i_{a_m}^{Grid}$) [14]. This approach represents the novel implementation

of an RLS approach based on coordinated DERs. Hence, if $i_{na_m}^{Grid}$ is distributively compensated, which allows for the shape of the MG as a resistor (i.e., from the grid perspective), the PCC currents will only present linear harmonics according to the equivalent conductance seen at that node.

A. Generalized Current-Based Control for RLS Operation

The GCBC is formulated considering in-phase (‖) and quadrature (⊥) components of currents from the DERs and the currents flowing through the MG PCC. No load currents need to be measured. The GCBC operation relies on four main tasks: *i*) local evaluation of electrical quantities; *ii*) selection of RLS reference peak currents at the CC; *iii*) GCBC processing at the CC; and *iv*) local current reference setting.

First, the local evaluation of electrical quantities occurs as follows. At each *j*-th DER, and also at the CC, the detection of the magnitudes (i.e., peak values) of the in-phase and quadrature output currents (i_m^o) is required by the GCBC, as in Fig. 2(a) and Fig. 2(b). This procedure is done for each *h* order (i.e., fundamental and harmonics) desired to be controlled. While controlling active and reactive currents and performing harmonic mitigation, *h* stands as *h = 1,3,5,7,..., H*, where *H* is the highest order. In general, the harmonics (i.e., even and odd terms) with the highest amplitudes are the ones considered for the GCBC. Also, the CC is the one responsible for selecting *h*.

The decomposition of the *m*-phase peak current terms ($I_{h\|_m}$ and $I_{h\perp_m}$) from DERs and PCC occurs based on a discrete Fourier transform (DFT) and based on unitary sinusoidal signals that are in-phase and quadrature to voltages (i.e., $x_{h\|_m}$ and $x_{h\perp_m}$). These sinusoidal signals are obtained based on a phase-locked-loop (PLL). A thorough explanation of this step is found in [20]. Besides, since heavily distorted grid voltages may exist, the considered PLL should be robust to such a condition. The same PLL method from [20] is adopted in this paper, based on moving average filters.

The second step of the GCBC occurs only at the PCC, aiming at choosing the adequate grid peak currents ($I_{h\|_m}^{Grid}$ and $I_{h\perp_m}^{Grid}$) to be shared by the DERs. As seen in Fig. 2(b), when γ_{RLS} is set to 1, the Fryze's active current decomposition leads to the calculation of $i_{na_m}^{Grid}$ as in (1). In (1.b), *P* is the average three-phase active power at PCC. Moreover, $\boldsymbol{V}_{col}^{Grid}$ is the collective [14] PCC voltage given by (1.c), where V_{RMSm}^{Grid} is the *m*-phase rms voltage. Note that this formulation is straightforwardly applied to single-phase systems without modifications.

$$i_m^{Grid} = i_{a_m}^{Grid} + i_{na_m}^{Grid} \tag{1.a}$$

$$i_{na_m}^{Grid} = i_m^{Grid} - i_{a_m}^{Grid} = i_m^{Grid} - \frac{P}{(\boldsymbol{V}_{col}^{Grid})^2}.v_m^{Grid} \tag{1.b}$$

$$\boldsymbol{V}_{col}^{Grid} = \sqrt{(V_{RMSa}^{Grid})^2 + (V_{RMSb}^{Grid})^2 + (V_{RMSc}^{Grid})^2} \tag{1.c}$$

Now, as seen in Fig. 2(b), the local evaluation of quantities at the CC decomposes $i_{na_m}^{Grid}$. As output, the reactive peak current ($I_{1\perp_m}^{Grid}$) is obtained, along with harmonic peak currents non-proportional to the voltages ($I_{h\|_m}^{Grid}$ and $I_{h\perp_m}^{Grid}$) for *h > 1*.

At the third step of the GCBC, each *j*-th inverter is required to periodically send to the CC a data packet consisting of the in-phase and quadrature peak values of the *h* order currents of their PoCs ($I_{h\|_m}^{DER}$ and $I_{h\perp_m}^{DER}$), as well as their installed nominal ratings ($I_{nom_m}^{DERj}$), their actual capability to inject active current ($I_{max_m}^{DERj}$), and their capability to absorb active current ($I_{sto_m}^{DERj}$) (if energy storage is present). Then, at the beginning of a control cycle *k*, the CC calculates the total (i.e., superscript "*t*") peak currents processed by all DERs, as in (2). The same calculation applies for the DERs' capabilities (i.e., $I_{nom_m}^{DERt}$, $I_{max_m}^{DERt}$, and $I_{sto_m}^{DERt}$).

$$I_{h\|_m}^{DERt}(k) = \sum_{j=1}^{J} I_{h\|_m}^{DERj}(k) \tag{2.a}$$

$$I_{h\perp_m}^{DERt}(k) = \sum_{j=1}^{J} I_{h\perp_m}^{DERj}(k) \tag{2.b}$$

Since the CC is placed at the PCC, it is responsible for calculating the in-phase and quadrature peak currents currently being drawn from the upstream grid ($I_{h\|_m}^{Grid}$ and $I_{h\perp_m}^{Grid}$). However, if RLS is desired, the terms $I_{h\|_m}^{Grid}$ and $I_{h\perp_m}^{Grid}$ come from the second step of the GCBC. Thus, having such information, the coordinated control of DERs is determined by defining the reference peak currents that need to be shared among them in the next control cycle, "*k+1*", namely $I_{h\|_m}^{*}$ and $I_{h\perp_m}^{*}$. Such references are computed for each in-phase and quadrature *h* orders, given by (3). Note in (3) that $I_{1\|_m}^{Grid*}$ and $I_{1\perp_m}^{Grid*}$ are the active and reactive current terms desired to circulate at the PCC in *k+1*, respectively, which the CC sets. Such grid current references allow the MG to act as a single-controllable entity for active and reactive power. Moreover, (3) is valid due to the limited size of the MG since the low X/R line impedance feature does not cause significant phase shifts among voltage nodes.

$$I_{h\|_m}^{*}(k+1) = I_{h\|_m}^{Grid}(k) + I_{h\|_m}^{DERt}(k) - I_{h\|_m}^{Grid*}(k+1) \tag{3.a}$$

$$I_{h\perp_m}^{*}(k+1) = I_{h\perp_m}^{Grid}(k) + I_{h\perp_m}^{DERt}(k) - I_{h\perp_m}^{Grid*}(k+1) \tag{3.b}$$

Finally, to steer DERs to provide current sharing while respecting their current capacities, scaling coefficients, $\alpha_{h\|_m}$ and $\alpha_{h\perp_m}$ are determined for all current terms to be controlled (i.e., respective to the *h* orders). Such coefficients are given by (4), and they consider the overall peak current capability of the network ($\sqrt{\Delta I_m}$). Later, the calculated coefficients are broadcasted to all DERs, for adjusting their current injections.

$$\alpha_{h\|_m} = \frac{I_{h\|_m}^{*}(k+1)}{\sqrt{\Delta I_m}} \quad and \quad \alpha_{h\perp_m} = \frac{I_{h\perp}^{*}(k+1)}{\sqrt{\Delta I_m}} \tag{4}$$

Each of these terms is responsible for controlling a current parcel, on which, for instance, $\alpha_{1\|_m}$ and $\alpha_{1\perp_m}$ relate to the active and reactive current terms, respectively, while higher *h* orders are used to mitigate harmonics. In addition, such coefficients are within the range of [-1, 1], which represents: power absorption/storage (if $\alpha_{1\|_m}$ is negative) or active power injection (if positive, i.e., $\alpha_{1\|_m} > 0$); capacitive (if $\alpha_{1\perp_m}$ is negative) or inductive behavior (if positive). Sequential logic is used for each α_{h_m}, being processed up to the highest order (*H*) (i.e., following $\alpha_{1\|_m}$, $\alpha_{1\perp_m}$, $\alpha_{3\|_m}$, …, $\alpha_{H\|_m}$, $\alpha_{H\perp_m}$). Yet, to avoid overcurrent, the per-phase MG capability ($\sqrt{\Delta I_m}$) is recalculated sequentially upon the processing of each α_{h_m} coefficient targeted on the control action. For instance, after calculating $\alpha_{1\|_m}$, the capability for $\alpha_{1\perp_m}$ is $\Delta I_m = (I_{nom_m}^{DERt})^2 - (I_{1\|_m}^{DERt})^2$, where $I_{1\|_m}^{DERt}$ is limited to $I_{max_m}^{DERt}$ or $I_{sto_m}^{DERt}$ if injection or storage of active current is intended, respectively.

As the last step of the GCBC strategy, to allow the *J*-DERs to inject the desired currents, their time-domain *m*-phase reference current (i_m^{j*}) is locally built. Such currents are set based on (5), where the reference peak currents, $I_{h\parallel_m}^{j*}$ and $I_{h\perp_m}^{j*}$ At each *h* order, are multiplied by the respective unitary in-phase and quadrature signals. Note that the peak references are attained from α_{h_m} and the local capability of each DER ($\sqrt{\Delta I_m^j}$), which is calculated sequentially, as done at the CC.

$$i_m^{j*} = \sum_{h=1,3,5,\dots}^{H} \left(\alpha_{h\parallel_m} \cdot \sqrt{\Delta I_m^j}\right) \cdot x_{h\parallel_m}^j + \left(\alpha_{h\perp_m} \cdot \sqrt{\Delta I_m^j}\right) \cdot x_{h\perp_m}^j \quad (5)$$

IV. Simulation Results

Herein simulation results demonstrate the proposed RLS strategy. The MG testbench presented in Fig. 1 is implemented in Matlab/Simulink, according to the model from [18]. Three three-phase current-controlled DERs are considered, as in Figs. 1 and 2. Their inner current loops use proportional-repetitive (PRep) controllers as in [24]. Constant voltage sources feed the DC buses of the DERs. The DERs' parameters are in Table I. Several linear and non-linear loads (see Fig. 1) represent the circulation of active, reactive, and harmonic currents. The MG's non-linear power is around 20% of the overall apparent power of the loads. A resonant load is also placed at the PCC when desired. This load comprises a line impedance segment and a delta-formed capacitive bank connected to the PCC through the circuit breaker CB_1.

Concerning the GCBC operation, the selected harmonic frequencies shared by the DERs in simulations are set to the fundamental and odd orders, from the 3rd up to the 13th, since they are the most significant ones in the load currents. The data transmission between the CC and DERs occurs once at each fundamental cycle (i.e., 20 ms). Moreover, slower data transmission speeds could be adopted, only resulting in longer settling times, not impairing system stability, as shown in [20].

Two case studies are presented. The first case considers the MG operating under distorted voltages imposed by the main grid. The proposed approach is demonstrated to share currents, offering RLS-based compensation of reactive and harmonic currents to achieve high PF operation. Additionally, the active current sharing capability is shown. As a second simulation case, the resonant load is enabled, and it is shown that the proposed RLS approach supports the damping of harmonic resonances. Finally, a comparison with an SCS approach depicts the advantage of the RLS method.

A. Case 1: Distorted Voltages Imposed by the Grid

For this case, the upstream grid imposes distorted voltages at the primary side of the distribution transformer. Thus, resulting in nonlinearities of the 7th harmonic order, with 6% of amplitude in relation to the fundamental voltages (e.g., for phase *a*, $v_a^{Grid} = 400.\cos(\omega.t) + 24.\cos(7.\omega.t)$). The MG operates to achieve high PF at the MG PCC, and the results are depicted in Fig. 3, being split into four intervals. The PF is calculated as in [16] (i.e., as defined in Section I).

First, at Interval I in Fig. 3(a) and 3(b), it is shown how the voltages are distorted at the PCC. This case considers the DERs idling (i.e., not processing any currents). Consequently, only the load currents are seen at the PCC, being considerably distorted and phase-shifted related to the voltages. At this interval, the total harmonic distortion of the phase currents (THD_i) is 7.70%, with PF = 0.93. Fig. 4 shows that the harmonic spectrum of the PCC currents has several components. The most significant ones are the 5th, 7th, 11th, and 13th orders, being the 7th order the only one existing in the grid voltages (see supplementary material file for additional quantitative details).

TABLE I
MG and DERs' Parameters Used for Simulations

Feature	Specification
LV MG line voltage (fundamental) and freq.	400 V @ 50 Hz
DERs rated apparent power [A_{DER1}, A_{DER2}, A_{DER3}]	[35, 20, 35] kVA
DERs DC link voltage (V_{DC})	750 V
LCL filter: inverter- (L_i) and grid-side (L_g) inductor	3.5 and 1.5 mH
LCL filter: capacitor (C_f)	2.2 µF
LCL filter active damping gain (K_{damp})	4.8 pu
Switching (f_{sw}) and sampling frequencies (f_s)	15 kHz
PRep controller: proportional and repetitive gain	0.26 and 0.28 pu

At Interval II, the GCBC is initiated, and the DERs are coordinated to share the reactive and harmonic currents seen at the PCC, following the RLS approach. Note in Fig. 3(a) and 3(c) that the DERs promptly change their current injections, starting to process fundamental and harmonic currents. Besides, such operation occurs proportionally to their nominal capabilities (e.g., see in Fig. 5 that DER_1 and DER_3 inject the same collective [14] currents and that DER_2 injects a collective current about 57% smaller, given that $A_{DER2} \approx 0.57 x A_{DER1}$). Since DERs follow the RLS approach, the PCC currents are in phase and resemble the voltage waveforms. Fig. 4 shows that the harmonic spectrum of the PCC currents mostly comprises fundamental and the 7th orders. Also, the fundamental is reduced due to the reactive compensation.

If an SCS approach was implemented for Interval II, the PF at PCC would not be unity (e.g., a PF=0.982 is obtained for this case). However, since the proposed RLS approach shapes the MG to synthesize a resistor, the PF at the PCC becomes 0.999. This result indicates that mostly active power flows through the PCC. Consequently, this supports the operation of the upstream grid by achieving controllable MG power flow also under distorted voltages, with null reactive and non-linear power dispatch. Although harmonic currents non-proportional to the voltages are compensated, it is reinforced that the RLS approach leads to distorted currents at the PCC. For this case, the THD_i is 6.29%, 6.31%, and 6.32%, respectively, for phases *a*, *b*, and *c*. Figs. 3(c) and 4 show that only the 7th harmonic order exists during Interval II.

At Interval III in Fig. 3(a) and 3(d), the dynamic response of the proposed strategy is shown. At 0.6s, a load step occurs by suddenly switching off the circuit breakers CB_2 and CB_3, which connect the non-linear loads in the buses *B16* and *B18* (see Fig. 1), respectively. Note in Fig. 3(a) that the PCC currents promptly change despite the abrupt disconnection of the loads, although neither overcurrent nor overvoltage occurred at the PCC and DERs' PoCs. In addition, since the GCBC communicates with DERs each 20 ms, the shared currents started to be readjusted only after one fundamental cycle. Moreover, after two more cycles, a steady-state is reached,

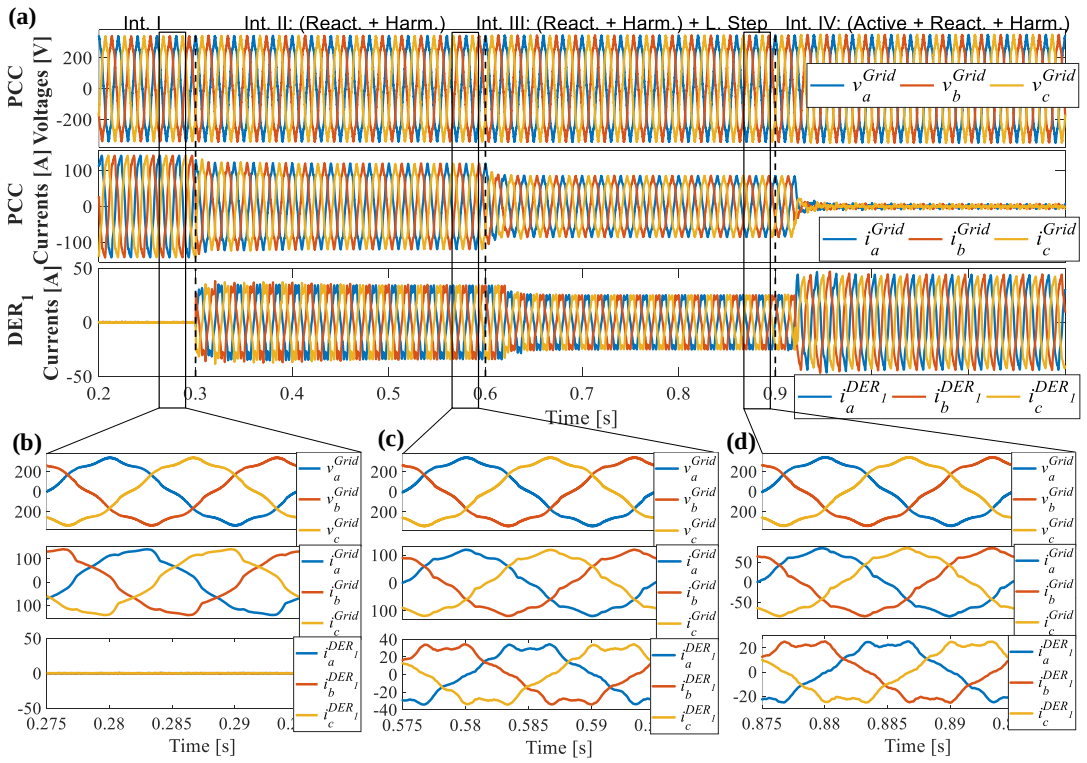

Fig. 3. Simulation results of the RLS-based GCBC approach for Case 1: high PF operation. (a) From top to bottom: PCC voltages and currents and DER_1 currents; (b) Zoom-in-view of Interval I; (c) Zoom-in-view of Interval II; and (d) Zoom-in-view of Interval III.

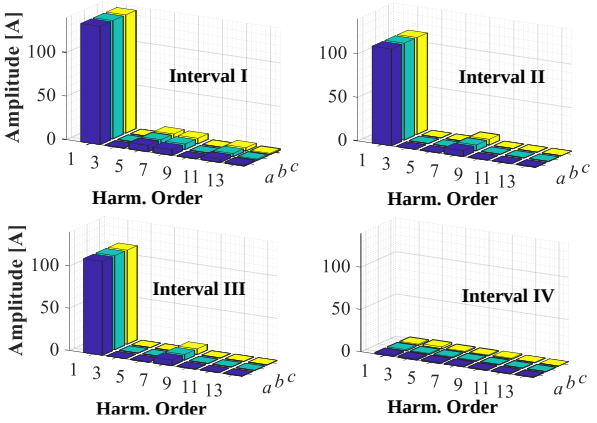

Fig. 4. Harmonic spectrum of the PCC currents in Case 1 – Fig. 3.

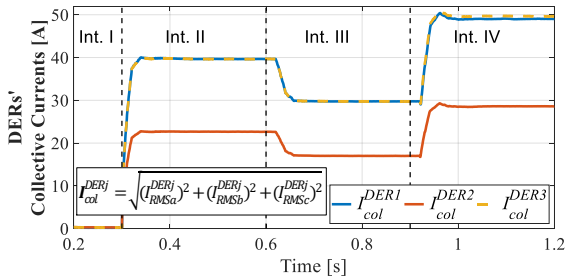

Fig. 5. DERs' collective currents [14] for intervals in Fig. 3.

maintaining the features of the RLS approach. Thus, currents are still in phase with voltages (see Fig. 3(d)), and mostly harmonics proportional to the voltages exist. Fig. 4 reassures that only the 7th order remained at the PCC, as in Interval II.

For the last scenario (i.e., Interval IV), the active sharing capability under distorted voltages is shown, having the results shown in Fig. 3(a). At 0.9s, the GCBC is set to control the active current dispatch at the PCC while also compensating for reactive and harmonic currents. The results show that the GCBC can support such functionality, quickly adjusting the current injections of DERs to process active, reactive, and harmonic components. From Figs. 3(a) and 4, it is seen that all current terms are practically null at the PCC. Note that if the DERs share the most significant current terms flowing through the PCC, the MG operates (i.e., in steady-state) under full self-consumption mode. The self-consumption service is commercially found in local controllers of DERs. Besides, it is deemed important since it supports optimized electricity planning of LV grids [17]. In this paper, such a concept is expanded to the MG perspective, considering active power control and targeting reactive and harmonic control.

B. Case 2: Coordinated RLS for Resonance Damping

Now, the capability of the proposed coordination of DERs on supporting the damping of harmonic resonances is discussed. Results are presented in Figs. 6 and 7, and Table II. For this simulation, the capacitor bank of the resonant load placed at the PCC is added to the MG by switching on CB_1 (see Fig. 1). This type of passive compensator is usually placed close to the distribution transformer to support the regulation of voltage profiles and purposes of reactive power compensation [4]. Nonetheless, the interactions of this capacitive filter with line impedances and non-linear loads may deteriorate voltage quality if resonances are triggered. To demonstrate that, a small amount of 1 % of the 7th harmonic order is added to voltages (i.e., in relation to fundamental voltage, similar to Case 1).

At Interval I in Fig. 6(a) and 6(b), the harmonic resonances caused by the interactions within the MG are demonstrated. All

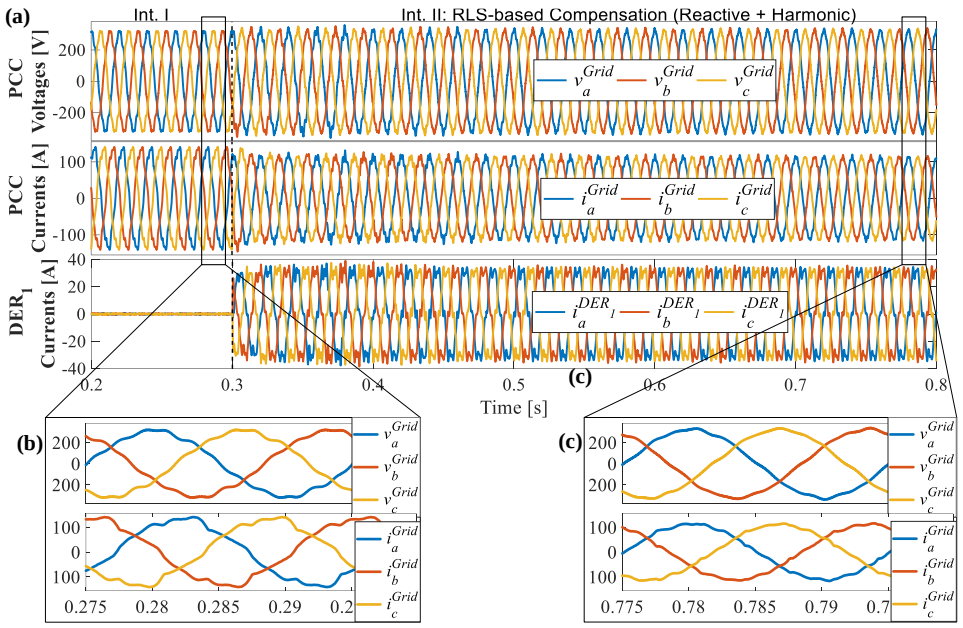

Fig. 6. Simulation results of the proposed RLS approach for Case 2: resonance damping. (a) From top to bottom: PCC voltages and currents and DER_1 currents; (b) Zoom-in-view of PCC voltages and currents at Interval I; (c) Zoom-in-view of PCC voltages and currents at Interval II.

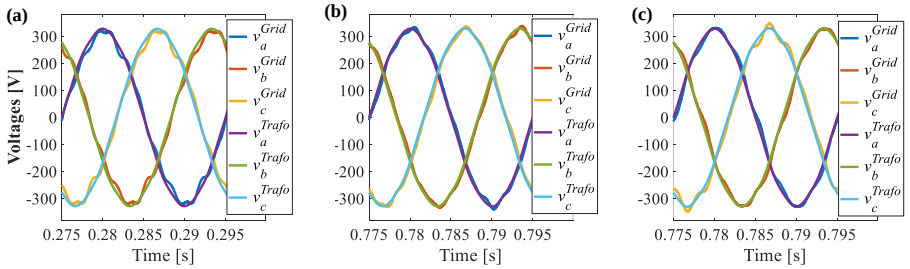

Fig. 7. Comparison results for Case 2 - Voltages at the distribution transformer and the PCC for: (a) Int. I; (b) Int. II - RLS; (c) Int. II - SCS.

TABLE II

Voltage amplitudes (i.e., peak values [V_{pk}]), PF, and THD_v for the PCC and the secondary side of the MG transformer in simulation Case 2.

		Transformer Voltages			PCC Voltages (Int. I)			PCC Voltages – RLS (Int. II)			PCC Voltages – SCS (Int. II)		
Phase		***a***	***b***	***c***	***a***	***b***	***c***	***a***	***b***	***c***	***a***	***b***	***c***
Harmonic Order	1	325.59	325.58	325.58	312.54	312.54	312.54	324.31	324.22	324.26	324.70	324.53	324.86
	3	0.01	0.01	0.02	0.01	0.02	0.02	0.14	0.20	0.29	0.39	0.33	0.63
	5	0.04	0.03	0.03	9.54	9.54	9.53	0.50	0.43	0.42	0.79	0.18	0.62
	7	3.40	3.38	3.39	5.59	5.63	5.55	6.75	6.61	6.82	11.37	11.00	10.26
	9	0.05	0.08	0.12	0.27	0.08	0.22	0.62	0.99	1.61	6.06	6.64	12.64
	11	0.15	0.16	0.18	10.71	10.67	10.75	1.82	1.92	2.13	0.93	1.46	1.0
	13	0.05	0.08	0.10	1.44	1.46	1.47	0.54	0.84	1.10	0.41	0.65	0.96
THD_v [%]		1.05	1.04	1.05	4.96	4.96	4.97	2.47	2.44	2.53	4.02	4.02	5.06
PF			0.92			0.93			0.99			0.98	

DERs are disabled at this instant. It is seen that voltages are significantly distorted, with a much higher THD_v value than the 1 % of harmonic pollution inserted at the voltages. Table II shows that the THD_v value increases from about 1 % to approximately 5 % at the PCC due to the resonances. Moreover, even though only the 7^{th} order was added to the voltages at the secondary side of the transformer, a significant amount of the 5^{th}, 7^{th}, $11^{th,}$ and 13^{th} harmonics also exist at the PCC voltages (see Table II). In Fig. 7(a), the transformer and PCC voltages are visually compared, reassuring the effects of the triggered resonances. Yet, Fig. 6(b) also shows that the PCC currents are still phase-shifted and distorted (i.e., with multiple harmonics), and a low PF occurs.

For the second interval in Fig. 6, the GCBC is enabled at 0.3s, commanding the DERs to share the PCC reactive and harmonic currents based on the RLS approach. By having inverters sharing the harmonic currents, the PCC voltages start responding without causing overvoltage (see Fig. 6(a)). Likewise, the PCC currents do not suffer overcurrent. Note that, as the PCC voltages dynamically change due to the effects of the distributed compensation, the GCBC keeps on adjusting the current sharing until a steady state is obtained after around 0.4s.

As a result, the currents resemble the voltage waveforms (see Fig. 6(c)), increasing the damping capability of the MG due to the resistive shaping [3] and concomitantly reaching a high PF.

The direct consequence of shaping the MG as a selective resistor is that most of the harmonic resonances are suppressed, as seen in Table II. Note that a considerable amount of the 5th, 11th, and 13th harmonic distortions are damped. Moreover, the fundamental component is restored to 99 % of its nominal value (e.g., for phase *a*, the voltage amplitude is 324.31 V, compared to 325.59 V at the secondary side of the transformer). Fig. 7(b) shows that the PCC voltage waveforms are now more similar to those from the transformer secondary side. A final THD_v of approximately 2.5% is obtained for the PCC phase voltages, representing a significant improvement from the previous 5% value. Interval II presented THD_v and THD_i below the limits indicated by the IEEE 519-2014 standard (see supplementary material file). However, it is highlighted that the proposed coordination based on RLS aims at compensating unwanted current components, supporting the damping of harmonic resonances in voltages as a direct consequence. If a harmonic-free scenario is desired, upon having the grid imposing distorted voltages, active compensators can be placed at the MG PCC.

Finally, another comparative study of the proposed RLS-based coordination against the SCS approach from [20] is presented. The GCBC strategy is then adjusted, as seen in Fig. 2(b), to share all the harmonic currents of the loads (i.e., terms proportional and non-proportional to the voltages). By striving to obtain sinusoidal currents upon the same scenario accounting for resonances (i.e., as in Fig. 6(c)), the suppression of harmonic distortions is minimized. For instance, in Table II, the voltage amplitude of the 5th, 11th, and 13th orders is reduced comparing to Interval I (i.e., respectively by around 91%, 86%, and 71%). Nevertheless, compared to the RLS scenario, the 7th order was 82% higher. Moreover, additional distortions at the 9th order were significantly triggered by using SCS. Thus, this result proves that the SCS approach is less effective than the proposed RLS technique for what concerns resonance damping. Fig. 7(c) visually demonstrates that voltages are more distorted when SCS is selected, presenting a THD_v of around 4 % for phases *a* and *b* and 5 % for phase *c*. Consequently, given the considered scenario, simulations show that the RLS approach improved the damping capability in about 38%, 39%, and 50% for phases *a*, *b*, and *c*, respectively, compared to SCS. Such results consider the THD_v as the figure of merit (see Table II; e.g., the THD_v for phase *c* was 5.06% and 2.53% for the SCS and RLS cases, respectively, leading to such a 50% improvement).

V. Experimental Results

A laboratory-scale single-phase MG prototype has been assembled to verify the feasibility of the proposed RLS-based coordination of inverters. Such a prototype is seen in Figs. 8(a) and 8(b), and its equivalent circuit is shown in Fig. 8(c). The MG comprises two single-phase DERs (i.e., DER_1 and DER_2) composed of full-bridge SEMIKRON® inverters, considering LC output filters (i.e., with 3.5 mH and 2.2 μF). The DERs' nominal power are 1.85 and 2.5 kVA, respectively for DER_1 and DER_2, resulting in a proportion ratio of r_{DERs} = 1.85/2.5 = 0.74. An F28335 DSP is used to implement the proportional-resonant (PR) current controllers of DERs, as in [25]. The sampling (f_s) and switching frequencies (f_{sw}) are 12 kHz due to the DSP's computational constraints. It is highlighted that, regardless if f_s and f_{sw} are 12 or 15 kHz, similar performance is obtained for simulations and experiments (see supplementary material file). The PR controllers are tuned at the fundamental, 3rd, and 5th orders. The values of the proportional (KP_i) and harmonic (KI_h) gains are 0.20 and 358 pu. DERs' DC links are fed by DC voltage sources with 270 V_{dc}.

A REGRATRON® bidirectional AC voltage source emulates the upstream grid. As seen in Fig. 8(c), three loads are considered, being one inductive (L_2 = 40 mH) and one non-linear (L_3), which is comprised of a diode bridge rectifier having an inductor (5 mH) at its AC side and a capacitor bank (2.35 mF) in parallel with a resistor (41.8 Ω) at its DC side. An IT8616 electronic load (L_1) is also used, emulating a constant resistor with 16 Ω. The MG's non-linear power is around 27% of the overall apparent power of the loads. Line impedances exist in the MG, being $Z_{L1} = Z_{L2} = Z_{L3} = Z_{L4} = 2_x Z_{L5} = 0.02 + j0.188$ Ω. The proposed control strategy processed by the CC of the MG is also implemented within the DSP, considering data transmission rate with DERs of 0.16 ms. The GCBC is set to control the fundamental, 3rd, and 5th harmonic orders.

Experimental results are presented in Figs. 9, 10, and 11, and they consider two voltage scenarios to demonstrate the RLS feature and control capabilities of the proposed approach. First, the fundamental grid voltage is set to 127 V_{rms} at 60 Hz (i.e., as a common single-phase Brazilian LV grid [19]), with 15 % of the 5th harmonic (i.e., 19 V_{rms}). For the second scenario, such a 15 % voltage distortion is changed from the 5th to the 3rd order.

In Fig. 9(a), the PCC voltage and current are seen when DERs are idling for the scenario. Note that the current is phase-shifted (see phase angle in Fig. 9(a)) and presents distortions non-proportional to the voltage. The *P* and *Q* powers, calculated as in [16], and the amplitude of the PCC current harmonics are in Table III. They indicate low PF operation, regardless of voltages presenting distortions at the 3rd or 5th harmonics.

Then, in Fig. 9(b), the first experimental result with the RLS-based GCBC is shown when the strategy is enabled, allowing the DERs to share the reactive and harmonic currents. Note that the strategy can steer the DERs in proportion to their ratings. For instance, DER_1 processes 4.5 A_{rms} and DER_2 6.1 A_{rms}, which gives r_{DERS} = 0.73, matching the expected proportion of 0.74. As a result, the PCC current resembles the voltage, presenting negligible phase deviation, indicating operation under high PF (i.e., 0.99, see Table III). A second case is shown in Figs. 9(c) and 9(d), on which CB_{L2} switches off the inductive load L_2. It is seen in Fig. 9(c) that the MG smoothly transits the load step as the GCBC adjusts the DERs' injections, reaching steady-state in Fig. 9(d) with performance similar to Fig. 9(b) (see Table II), also presenting r_{DERS} = 0.72.

Now, the load L_2 is switched on again, and in Figs 10(a) to and 10(c), a dynamic change in the voltage distortion is abruptly emulated. Note in Figs. 10(a) and 10(b) that the changes in voltage and currents for the PCC and at DERs occur without causing any overvoltage or overcurrent. In addition, as seen in Fig. 10(c), the DERs reach steady-state operation after a few cycles (i.e., about 14 cycles). This situation occurred due to the dynamics of the GCBC algorithm, of the rms calculation required for (1.c) and (1.b), and due to the transient response of the current controllers. Fig. 10(c) shows that the strategy is

again able to shape the MG PCC to emulate a resistor without adjustments in the GCBC, and without decomposing voltages. Finally, Table III shows that the PCC current presents negligible phase shift and distortions at the same frequency of the voltage one (i.e., the 3rd order). This situation results in a high PF of 0.99, while DERs adequately present r_{DERS} = 0.73.

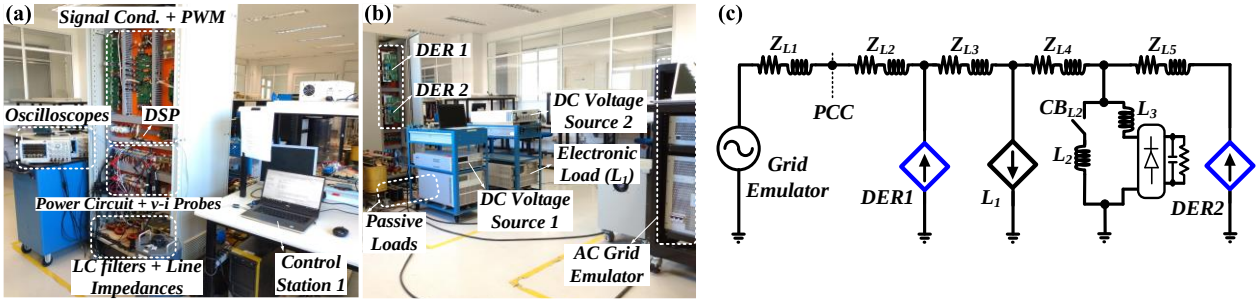

Fig. 8. MG prototype implemented for experiments: (a) front and (b) back views of the setup; (c) electric circuit of the single-phase MG.

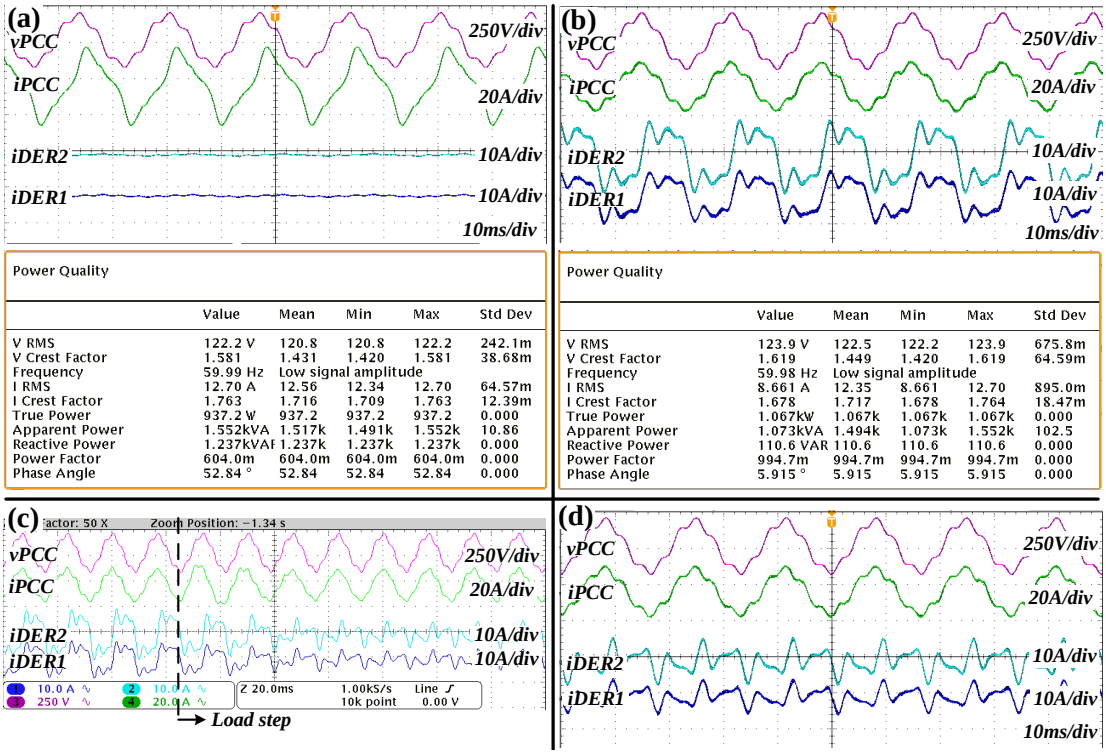

Fig. 9. Experiments of the RLS-based coordination of inverters under distorted voltages. From top to bottom: PCC voltage and current, DER_1 and DER_2 currents, and power quality indexes. (a) DERs turned off; (b) DERs turned on; (c) transition from (b) during load step; (d) steady state of (c).

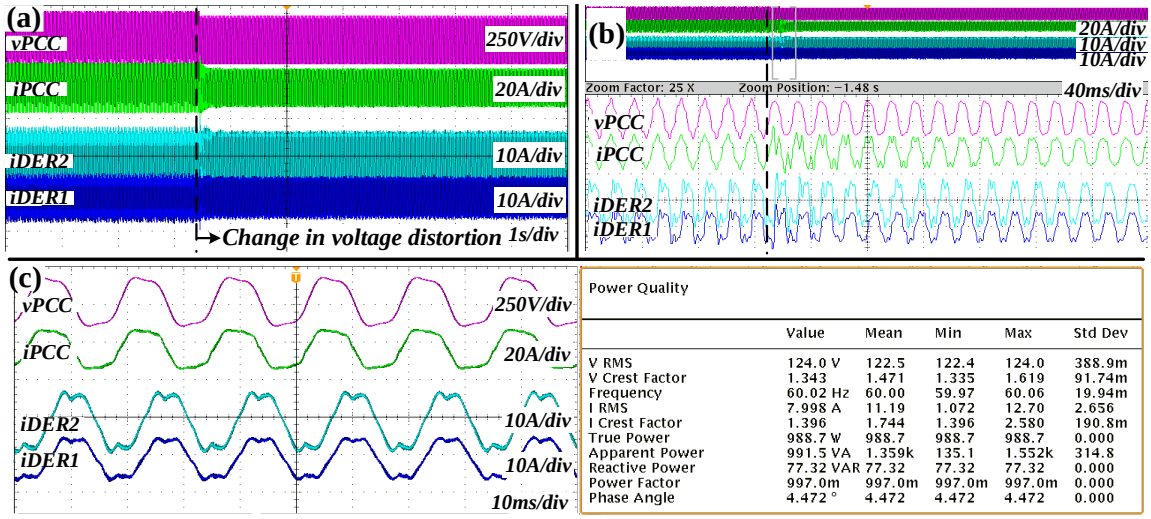

Fig. 10. Experiments of the RLS-based coordination of inverters with different voltage distortions. From top to bottom: PCC voltage and current, DER_1 and DER_2 currents. (a) Change in grid voltage distortion from the 5th to the 3rd harmonic; (b) zoom-in-view of (a); (c) steady state of (b).

TABLE III

CURRENTS, POWERS [16], PF, AND THD AT PCC DURING EXPERIMENTS.

	Harm.	DERs Off		Fig. 9(b)	Fig. 9(d)	Fig. 10(c)	Fig. 11
		Dist. 5th	*Dist. 3rd*				
Current [A_{RMS}]	1	12.1	12.0	8.54	8.66	7.88	0.42
	3	2.78	1.32	0.15	0.08	1.16	0.15
	5	1.17	0.62	1.31	1.32	0.05	0.05
	7	0.15	0.27	0.17	0.11	0.26	0.11
	9	0.13	0.15	0.09	0.07	0.15	0.14
***P* [W]**		940	911	1064	1086	988	-55
***Q* [VAR]**		1122	1095	-1	9	6	-15
PF		0.62	0.63	0.99	0.99	0.99	0.0
THD_i [%]		24.0	12.0	15.7	15.1	15.4	-
THD_v [%]		14.9	16.7	15.1	15.1	15.4	15.8

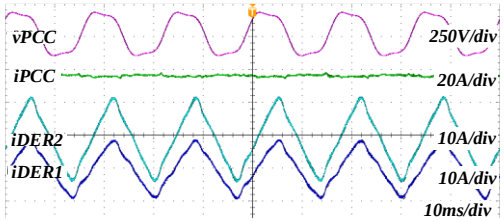

Fig. 11. Full self-consumption mode for the MG under distorted voltages.

A final experiment is shown in Fig. 11 to certify the capability of the GCBC also to share active currents under highly distorted voltages. Thus, the active, reactive, and harmonic (proportional and non-proportional) currents are considered references. Note that the DERs inject the load currents proportionally (i.e., with r_{DERS} = 0.71), resulting in practically null current at the PCC (see also practically null *P* and *Q* powers in Table III). Such a result proves that the MG full self-consumption mode is supported by the GCBC as well.

VI. CONCLUSION

This paper presented a model-free control strategy to coordinate distributed DERs existing in an interconnected LV MG, aiming to shape it to behave as a resistor at selected harmonic frequencies at the PCC. The approach is based on the RLS concept, being integrated into the GCBC strategy, allowing the possibility to automatically compensate current harmonics non-proportional to voltage distortions imposed by the upstream grid without implementing virtual impedance loops or decomposition of sequence components.

The simulation and experimental results showed that, by distributedly compensating non-active currents under such an RLS perspective, a high PF of 0.99 could be attained at the PCC, supporting higher energy efficiency for the distribution grid. Moreover, results showed that the approach supports active current sharing among DERs, allowing the MG to operate as a single-controllable entity, achieving full self-consumption mode under heavily distorted voltages.

The control approach is also capable of damping harmonic resonances triggered by interactions among grid and MG elements, supporting improved voltage quality (e.g., results showed that a per-phase THD_v as low as 2.4% was achieved under such scenario). Finally, for the considered MG testbench, up to 50% of improvement in resonance damping could be obtained in results comparing to an SCS strategy.

REFERENCES

[1] D. J. Hogan et al, "An Adaptive Digital-Control Scheme for Improved Active Power Filtering Under Distorted Grid Conditions," *IEEE Trans. Ind. Electron.*, vol. 65, no 2, pp. 988-999, Feb. 2018.

[2] J. He et al, "Analysis and Mitigation of Resonance Propagation in Grid-Connected and Islanding Microgrids," *IEEE Trans. Energy Conv.*, vol. 30, no 1, pp. 70-81, Mar. 2015.

[3] T. E. Zuniga, J. A. Pomilio, "Shunt Active Power Filter Synthesizing Resistive Loads," *IEEE Trans. Power Electron.*, vol. 17, Mar. 2002.

[4] A. Arguello, R. Torquato, W. Freitas, A. P. Feltrin, "A Graphical Method to Assess Component Overload due to Harmonic Resonances in Wind Parks," *IEEE Trans. Power Del.*, vol. PP, Aug. 2020.

[5] S. Devassy, B. Singh, "Performance Analysis of Solar PV array and Battery Integrated Unified Power Quality Conditioner for Microgrid Systems," *IEEE Trans. Ind. Electron.*, vol. PP, Apr. 2020.

[6] X. Wang et al, "Autonomous Control of Inverter-Interfaced DGs for Harmonic Current Filtering and Resonance Damping in an Islanded MG," *IEEE Trans. Ind. Appl.*, vol. 50, Jan. 2014.

[7] Y. Chen et al, "Fast Reactive Power Sharing, Circulating Current and Resonance Suppression for Parallel Inverters Using Resistive-Capacitive Output Impedance," *IEEE Trans. Power Electron.*, vol. 31, Aug. 2016.

[8] L. Zhou et al, "Harmonic Voltage Distortion Damping Method for Parallel-Connected LCL-Type Inverters in Islanded Operation," *IEEE Trans. Ind. Electron.*, vol. 66, no. 11, pp. 9032-9044, Nov. 2019.

[9] J. He et al, "Simultaneous Microgrid Voltage and Current Harmonics Compensation Using Coordinated Control of Dual-Interfacing Converters," *IEEE Trans. Power Electron.*, vol. 32, no. 4, Apr. 2017.

[10] Z. Zeng, R. Zhao, H. Yang, "Coordinated control of multi-functional grid-tied inverters using conductance and susceptance limitation," *IET Power Electron.*, vol. 7, no 7, pp. 1821-1831, Jul. 2014.

[11] A. M. S. Alonso et al, "Coordinated Control of Parallel Power Conditioners Synthesizing Resistive Loads in Single-Phase AC Microgrids," in *Proc. EPE ECCE Europe*, pp. 1-9, Sep. 2019.

[12] F. P. Marafao et al, "Multi-task control strategy for grid-tied inverters based on the CPT," *IET Renew. Power Gen.*, vol. 9, no 2, Feb. 2015.

[13] H. Akagi, "Control Strategy and Site Selection of a Shunt Active Filter for Damping of Harmonic Propagation in Power Distribution Systems," *IEEE Trans. Power Del.*, vol. 12, no 1, Jan. 1997.

[14] M. Depenbrock, "The FBD-Method, a Generally Applicable Tool For Analyzing Power Relations," *IEEE Trans. Power Syst.*, vol. 8, no 2, pp. 381-387, May 1993.

[15] L. S. Czarnecki, "What is wrong with the Budeanu concept of reactive and distortion power and why it should be abandoned," *IEEE Trans. Inst. Meas.*, vol. IM-36, no. 3, pp. 834-837, 1987.

[16] P. Tenti et al, "Conservative Power Theory, a Framework to Approach Control and Accountability Issues in Smart Microgrids," *IEEE Trans. Power Electron.*, vol. 26, no 3, Mar. 2011.

[17] SMA, *The self-consumption Bonus*. Jul. 2010. [Online] Available: https://www.sma.de/en/partners/knowledgebase/the-self-consumption-bonus.html

[18] *Benchmark Systems for Network Integration of Reneweable and Distributed Energy Resources*, CIGRE Task Force C6.04.02, 2009.

[19] H. K. M. Paredes et al, "Centralized Control Center Implementation for Synergistic Operation of Distributed Multifunctional 1Φ Grid-Tie Inverters in a MG," *IEEE Trans. Ind. Electron.*, vol. 65, Oct. 2018.

[20] A. M. S. Alonso et al, "A Selective Harmonic Compensation and Power Control Approach Exploiting Distributed Electronic Converters in Microgrids," *Int. J. Electr. Power Energy Syst.*, vol. 115, Sep. 2019.

[21] D. I. Brandao et al, "Model-Free Energy Management System for Hybrid AC/DC Microgrids," *IEEE Trans. Ind. Electron.*, vol. PP, Apr. 2020.

[22] J. P. Bonaldo et al, "Control of 1Φ Power Converters Connected to LV Distorted Power Systems with Variable Comp. Objectives," *IEEE Trans. Power Electron.*, vol. 31, no 3, pp. 2039-2052, Mar. 2016.

[23] A. M. S. Alonso et al, "Power- and Current-Based Control of Distributed Inverters in LV MGs: Considerations in Relation to Classic Droop Control," in *Proc. IEEE EVER Conf.*, Sep. 2020.

[24] P. Mattavelli, F. P. Marafao, "Repetitive-Based Control for Selective Harmonic Compensation in Active Power Filters," *IEEE Trans. Ind. Electron.*, vol. 51, Oct. 2004.

[25] S. Buso, P. Mattavelli, "Digital control in power electronics," 2nd Ed. Morgan & Claypool, 2015.

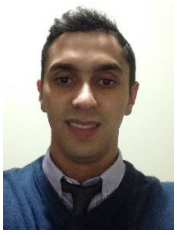

Augusto M. S. Alonso (S'16) received the B.S. degree in automation and control engineering from the Federal University of Ouro Preto, Brazil, in 2014, with a sandwich period as a BSMP Scholar at the University of New Mexico, USA, between 2012 and 2013. He received the M.S. degree in electrical engineering from the Sao Paulo State University (UNESP), Brazil, in 2018. Currently, he is a FAPESP Scholar working toward a double degree Ph.D. at UNESP and at the Norwegian University of Science and Technology (NTNU), Norway. In 2015 he was with Whirlpool Latin America/IEL/CNPq as an R&D engineer under the InovaTalentos fellowship. In 2019, he was a recipient of the Brazilian Power Electronics Society (SOBRAEP) award for the best M.S. thesis of the year. His main interests are coordinated control of converters, microgrid control, power quality, and energy policies. His is a member of IEEE and SOBRAEP.

Danilo I. Brandao (S'14–M'16) received the Ph.D. degree in electrical engineering from the University of Campinas, Brazil, in 2015. He was a visiting scholar at the Colorado School of Mines, USA, in 2009 and 2013, a visiting scholar at the University of Padova, Italy, in 2014, and a guest professor at the Norwegian University of Science and Technology, Norway, in 2018 and 2020. He is currently an assistant professor at the Graduate Program in Electrical Engineering with the Federal University of Minas Gerais, Belo Horizonte, Brazil. His main research interests are control of grid-tied converters and microgrids. He is a member of SOBRAEP.

Elisabetta Tedeschi (Senior Member, IEEE) received the M.Sc. degree (Hons.) in electrical engineering and the Ph.D. degree in industrial engineering from the University of Padua, Italy, in 2005 and 2009, respectively. From 2009 to 2011, she was a Postdoctoral Researcher with the Norwegian University of Science and Technology (NTNU), working on the grid integration of offshore renewable energies. She was a Researcher/Marie Curie Fellow at Tecnalia, Spain, from 2011 to 2013, where she worked as the Principal Investigator in the FP7-Sea2grid Project, related to the storage needs for the grid integration of wave energy converters. From 2013 to 2014, she was a Research Scientist at SINTEF Energy, and an Adjunct Associate Professor at NTNU. In 2014, she became a Full Professor within the offshore grid at NTNU. Since 2020, she has also been a Full Professor at the Department of Industrial Engineering, University of Trento, Italy. She has a core competence in the design and control of energy conversion and transmission and distribution systems, with a focus on offshore energy and power-quality issues. She has led and/or contributed to more than 15 national and international scientific projects and she has authored or coauthored two book chapters and more than 100 journals and conference papers in the field of marine energy and energy conversion systems.

Fernando P. Marafão (S'95–M'05) received the B.S. degree in electrical engineering from UNESP, Brazil, in 1998, and the M.Sc. and Ph.D. degrees from UNICAMP, Brazil, in 2000 and 2004, respectively. In 2002, he joined the Power Electronics Group, University of Padova, Italy, as a visiting student. In 2013, he joined the Colorado School of Mines, USA, as a Visiting Scholar on Autonomous and Intelligent Distributed Energy Systems. Since 2005, he has been with UNESP, as an Associate Professor with the Group of Automation and Integrating Systems. His current research interests include smart grid technologies, renewable energies, energy management and power theories. He is a member of SOBRAEP, SBA and IEEE.